Attenuation-corrected fluorescence extraction for image-guided surgery in spatial frequency domain

Bin Yang
Manu Sharma
James W. Tunnell

Attenuation-corrected fluorescence extraction for image-guided surgery in spatial frequency domain

Bin Yang, Manu Sharma, and James W. Tunnell
University of Texas at Austin, Department of Biomedical Engineering, Biophotonics Laboratory, Austin, Texas 78712

Abstract. A new approach to retrieve the attenuation-corrected fluorescence using spatial frequency-domain imaging is demonstrated. Both *in vitro* and *ex vivo* experiments showed the technique can compensate for the fluorescence attenuation from tissue absorption and scattering. This approach has potential in molecular image-guided surgery.

Molecular fluorescence-based image-guided surgery has played a significant role in the visualization of tumors[1] and has been demonstrated clinically for solid tumor removal.[2] Indeed, molecular fluorescence–based image-guided surgery will play an increasingly important role in the future of surgery. However, due to strong tissue absorption and scattering, the imaged fluorescence intensity can be distorted, obscuring the true fluorescence concentration and, thus, complicating the discrimination between fluorescently labeled tissues and that of normal or nonlabeled tissues. Here, we present a new technique to image tissue fluorescence free from the distortions of tissue scattering and absorption, called attenuation corrected fluorescence (ACF) imaging. ACF combines techniques developed for single-point (e.g., sensing) extraction of corrected fluorescence[3] and applies it to a whole image using spatial frequency-domain imaging (SFDI).[4,5]

In order to retrieve the true molecular fluorescence information from the measurements, the distortion, due to absorption and scattering at both excitation and emission wavelengths, must be corrected. Zhang et al. developed an approach to extract the undistorted fluorescence based on photon migration theory for fiber-optic probe based point measurement, and their algorithm is able to extract the undistorted fluorescence over a wide emission range, 370 to 700 nm.[3] The undistorted fluorescence, f_{xm}, is expressed as follows:

Address all correspondence to: James W. Tunnell, The University of Texas at Austin, Department of Biomedical Engineering, Biophotonics Laboratory, Austin, Texas 78712. Tel: +512.232.2110; Fax: +512.471.0616; E-mail: jtunnell@mail.utexas.edu

$$f_{xm} = \frac{F_{xm}}{\frac{1}{\mu_{sx}l}\left(\frac{R_{0x}R_{0m}}{\varepsilon_x\varepsilon_m}\right)^{1/2}\frac{R_x}{R_{0x}}\left(\frac{R_m}{R_{0m}}+\varepsilon_m\right)}, \quad (1)$$

where $\varepsilon = \exp(\beta) - 1$ and $\beta = S(1-g)$; F_{xm} is the raw fluorescence; R and R_0 represent diffusive reflectance with and without absorption, respectively; S and l are geometry-specific parameters; g is the anisotropy; and μ_{sx} is the scattering coefficient of the sample at the excitation wavelength. Subscripts m and x denote reflectance at the emission and excitation wavelengths. Only F_{xm} and R_m were measured directly, while the other parameters were calculated analytically using the diffuse reflectance model $R(\mu_a, \mu_s, g)$ of Zonios et al.[6] The sample optical properties were determined by applying the same analytical model in an inverse fashion. This approach is able to recover not only the shape of the spectrum but also the absolute intensity of the spectrum. Note that in order to apply the correction of Eq. (1), one must directly measure the fluorescence F_{xm}, the reflectance R, and the optical properties in order to determine the corrected fluorescence. Photon migration theory describes the behavior of photons in a turbid medium, which is applicable to both fiber-optic geometry and planar illumination. Wu et al. validated that the same approach can be applied to both fiber-optic-based measurements and wide-field measurements under planar illumination as long as the light delivery and collection geometry remain the same.[7] Of particular importance, the detected intensity at each pixel has contributions from its neighboring sources, and this particular source-detection geometry is accounted for by the constant S.

Translating this technique to an image is complicated by the lack of techniques to measure tissue optical properties over a full image field. Therefore, a commonly used correction in wide field is known as the ratio technique or F/R;[8] to compensate for scattering and absorption influences, the raw fluorescence signal (F) is divided by the reflectance (R) at the excitation wavelength. This approach is a simplified version of Eq. (1). The F/R technique has been employed in intraoperative fluorescence imaging system by Themelis et al.[9] However, this approach is limited as it does not account for the emission wavelength. Recently, Sagger et al. reported a model-based wide-field correction approach in the spatial frequency domain to evaluate protoporphyrin IX concentration from the skin.[10]

In this letter, we demonstrate the application of Zhang's photon migration model, developed for a point-measurement correction, on a two-dimensional (2-D) imaging field correction, which has the potential for molecular fluorescence image-guided surgery. We use a look-up table (LUT)-based SFDI technique[5] to rapidly measure the absorption coefficient (μ_a) and reduced scattering coefficient (μ_s') over the imaging field. By using the experimental LUT method, we are able to overcome the limitation of diffusion theory and extend SFDI to the visible spectrum, where the diffusion requirement for scattering dominance is not met. The SFDI system that we used is shown in Fig. 1. In SFDI, a 2-D spatially modulated sinusoidal pattern is generated on a digital micromirror device (Discovery 1100, TI) and the diffusely reflected images are captured with a non-cooled charge-coupled device (CCD) camera (Allied Vision, F145B). By projecting patterns with the same spatial frequency, but with phase offsets at 0, $2\pi/3$, and $4\pi/3$, three separate images with diffusely reflected intensities of I_1, I_2, and I_3, respectively, can be used to calculate the AC and DC components using Eqs. (2) and (3). The AC and DC components were further used as searching indices in the LUT to extract
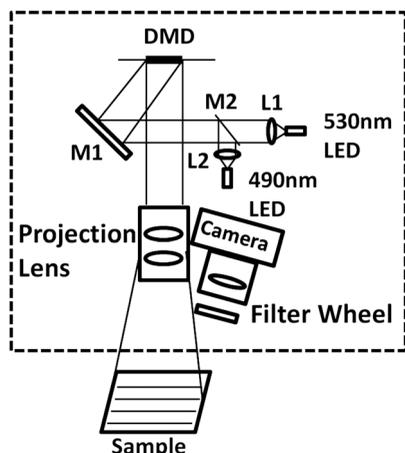
Fig. 1 Optical layout of ACF imaging system. Patterns are generated on the digital micromirror device, illuminated by LEDs, and projected by the projection lens to the sample. Filter wheel is used to select the wavelength and the imaging field is captured by a CCD camera.

the optical properties μ_a and μ_s'. We calculated the reflectance without absorption, R_{0m} and R_{0x}, by setting $\mu_a = 0$ and using the LUT in a forward manner. R_x was directly measured by filtering out the fluorescent signal, and R_m was obtained by measuring the reflectance at the emission wavelength. The parameters S and l are system-specific parameters. By adjusting parameters S and l, the corrected relative intensity and absolute intensity, respectively, can be calibrated. S was determined to be 0.22 by using calibration phantoms and remained constant. The scaling factor l was not determined as it does not affect the relative intensity retrieval. The anisotropy is medium specific and is usually obtained from well-established models.[11] The spatial frequency used in our study was 0.1/mm. Our previous study[5] showed that at this spatial frequency, the optical properties of the sample can be extracted with RMS errors of 5.7 and 2.9% for μ_s' and μ_a, respectively.

$$I_{AC} = \sqrt{2}/3 \left[\sqrt{(I_1 - I_2)^2 + (I_2 - I_3)^2 + (I_3 - I_1)^2} \right]. \quad (2)$$

$$I_{DC} = (I_1 + I_2 + I_3)/3. \quad (3)$$

We performed both *in vitro* and *ex vivo* experiments to investigate the efficacy of this approach. For the *in vitro* experiments, we fabricated tissue simulating phantoms using black India ink and 20% intralipid (Fresenius-Kabi) as the absorber and scatterer, respectively. Three sets of phantoms were prepared with $\mu_s' = 1.0$, 1.4, and 1.8 mm^{-1} at 530 nm. For each scattering value, the absorption coefficient was varied from $\mu_a = 0.05$ mm^{-1} to $\mu_a = 0.45$ mm^{-1} at 530 nm in $\mu_a = 0.1$ mm^{-1} increments. Therefore, a total of 15 combinations of μ_a and μ_s' values were measured. The concentration of fluorescein was kept constant throughout at 6.5 μg/ml. The anisotropy of intralipid was estimated as 0.9 at 365 nm and 0.85 at 530 nm based on the model of Flock et al.[12] These optical properties represent the biologically relevant range.

In this study, we used fluorescein (ACROS ORGANICS) as the fluorophore because of its high quantum yield and biological relevance.[2] In the *in vitro* phantom study, fluorescein was excited at 365 nm with a UV light-emitting diode (LED) (Thorlabs, M365L2) and peak emission occurred at ~520 nm.

Two bandpass filters with central wavelengths of 520 and 530 nm were used during the data acquisition under 365 and 530 nm illumination, respectively, in order to collect fluorescence F_{xm} and the reflectance at the emission wavelength R_m. A low-pass filter with a 420 nm cut-off was used to isolate the diffuse reflectance under illumination at the excitation wavelength. In the *ex vivo* tissue study, we chose a 490 nm LED as the excitation source to better suppress the autofluorescence and match the excitation wavelength that may be used in a clinical setting. A 500 nm low-pass filter was used to collect the diffuse reflectance from the excitation. All results in this letter were obtained using a 40% reflectance standard to normalize the signal and to correct for nonuniformities in the illumination field.

Figure 2 shows the results for phantom set with $\mu_s' = 1.4$ mm^{-1}. The phantoms without correction showed a substantial decrease in fluorescence intensity with increasing absorption including a fluorescence intensity drop of >80% at the highest level of absorption. This intensity decrease is qualitatively observed in the top row of Fig. 2(b). This attenuation was primarily due to strong absorption at both the excitation and emission wavelengths. Two correction techniques, F/R and ACF, were tested. After applying the ACF correction algorithm, the highest variation of fluorescence intensity was reduced to 9.7%. Thus, a much more uniform profile was recovered. The ACF correction outperformed the F/R technique over the entire range of optical properties. Figure 2(b) is a 2-D fluorescence image of the phantom set before and after ACF correction; significant improvement in the recovered fluorescence intensity is observed as all images maintain approximately the same intensity. The other two set of phantoms showed similar results.

To demonstrate the performance of this algorithm on real biological tissue, we prepared a model with minced chicken breast tissue of ~8 mm thickness. The center portion of the tissue model was homogenously mixed with fluorescein solution to mimic a tumor administrated with exogenous fluorophore [Fig. 3(a)]. Part of the tumor was covered with hemoglobin solution (Sigma-Aldrich, H0267) at a concentration of 10 mg/ml [Fig. 3(b)], to introduce additional absorption to mimic the case of fluorescence-guided surgical resection of a tumor. In order to apply the ACF correction algorithm, polystyrene beads with a nominal 1 μm diameter were used to simulate the scattering property of biological tissue using Mie theory, and the anisotropy was estimated as 0.9 and 0.91 at 490 and 530 nm, respectively.
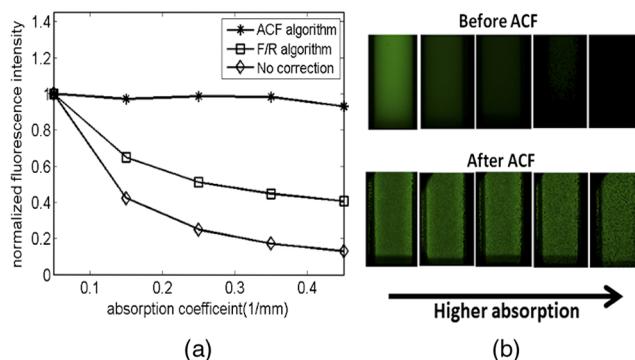
Fig. 2 (a) Normalized fluorescence intensity of *in vitro* tissue phantom with ACF correction, F/R correction, and no correction for phantom set with $\mu_s' = 1.0$ mm^{-1}. (b) The 2-D fluorescence image before and after the ACF correction.
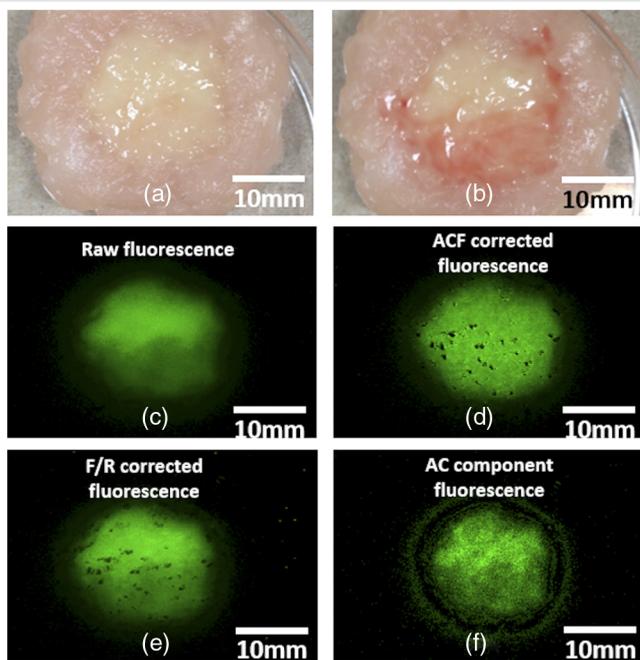
Fig. 3 Color image of tumor model (a), the tumor model partially covered with the blood (b), intensity image of the raw fluorescence under 490 nm illumination (c) and retrieved attenuation corrected fluorescence image (d) from the raw fluorescence, the corrected fluorescence (e) using F/R ratio method, and fluorescence image from AC component (f).

Figure 3(b) shows that only half of the tumor is visible to the naked eye, and the margin of the lower portion of the tumor is poorly defined due to the presence of blood. This is consistent with the raw fluorescence image [Fig. 3(c)]. We can see that the upper portion is bright, whereas the lower portion, covered with blood, is dull in comparison, due to hemoglobin absorption at the excitation and emission wavelengths. Therefore, in practice, this could result in only half of the tumor being excised. The application of the correction algorithm [Fig. 3(d)] results in a marked improvement as the whole tumor is now visualized. Furthermore, the corrected image accurately recovers the tumor margin and the uniform fluorescence intensity distribution. Excellent contrast can be observed between the background and the signal. The *ex vivo* results suggest that ACF is equally applicable to heterogeneous tissues and is able to yield consistent results as seen in the *in vitro* homogenous phantom study. For comparison purposes, Fig. 3(e) shows the result from the F/R ratio method. The attenuation is partially compensated by using the F/R ratio method; however, the intensity difference between the upper and lower portion of the tumor can still be observed. The black dots present in Fig. 3(d) and 3(e) are due to the specular reflection. Overall, these results are very promising as they indicate the potential of the ACF correction approach for image-guided surgery toward accurate identification of the entire tumor region.

Three issues should be noted. First, ACF is able to achieve the attenuation correction not because of optical sectioning, but because of the physical correction model used. The AC component image of the measurement obtained from optical sectioning[13] [Fig. 3(f)] was demonstrated to be different from the ACF corrected fluorescence [Fig. 3(d)]. Second, in our study, the samples are relatively flat, and no curvature correction algorithm[14] was employed. However, the curvature correction for

SFDI has been described in the literature[14] and could be implemented for the purposes of ACF imaging in future applications. Third, note that the diffuse reflectance at the excitation wavelength R_x was measured directly by using a low-pass filter. R_x is an estimate of the true value of the diffuse reflectance without fluorescence. With the presence of the fluorophore, the incident excitation light is partially absorbed by the fluorophore. The results from the tissue simulating phantom experiment indicated that the difference in diffuse reflectance with and without the fluorophore is <8% for a fluorophore concentration of 6.5 μg/ml. Therefore, the optical properties of the phantom at the excitation wavelength can still be estimated.

In conclusion, by taking advantage of the SFDI technique, we have demonstrated the efficacy of the attenuation corrected fluorescence extraction in an imaging field. Unlike other approaches, the performance is minimally affected by the underlying optical properties of the sample, and minimal knowledge of the sample optical property information is necessary to perform the correction. By employing the ACF correction method, the molecular image-guided surgery can yield better performance.

References

1. R. M. Hoffman, "The multiple uses of fluorescent proteins to visualize cancer in vivo," *Nat. Rev. Cancer* **5**(10), 796–806 (2005).
2. G. M. van Dam et al., "Intraoperative tumor-specific fluorescence imaging in ovarian cancer by folate receptor-[alpha] targeting: first in-human results," *Nat. Med.* **17**(10), 1315–1319 (2011).
3. Q. Zhang et al., "Turbidity-free fluorescence spectroscopy of biological tissue," *Opt. Lett.* **25**(19), 1451–1453 (2000).
4. D. J. Cuccia et al., "Quantitation and mapping of tissue optical properties using modulated imaging," *J. Biomed. Opt.* **14**(2), 024012 (2009).
5. T. A. Erickson et al., "Lookup-table method for imaging optical properties with structured illumination beyond the diffusion theory regime," *J. Biomed. Opt.* **15**(3), 036013 (2010).
6. G. Zonios et al., "Diffuse reflectance spectroscopy of human adenomatous colon polyps in vivo," *Appl. Opt.* **38**(31), 6628–6637 (1999).
7. J. Wu, M. S. Feld, and R. P. Rava, "Analytical model for extracting intrinsic fluorescence in turbid media," *Appl. Opt.* **32**(19), 3585–3595 (1993).
8. R. S. Kramer and R. D. Pearlstein, "Cerebral cortical microfluorometry at isosbestic wavelengths for correction of vascular artifact," *Science* **205**(4407), 693–696 (1979).
9. G. Themelis et al., "Real-time intraoperative fluorescence imaging system using light-absorption correction," *J. Biomed. Opt.* **14**(6), 064012 (2009).
10. R. B. Saager et al., "Quantitative fluorescence imaging of protoporphyrin IX through determination of tissue optical properties in the spatial frequency domain," *J. Biomed. Opt.* **16**(12), 126013 (2011).
11. W. F. Cheong, S. A. Prahl, and A. J. Welch, "A review of the optical-properties of biological tissues," *IEEE J. Quantum Electron.* **26**(12), 2166–2185 (1990).
12. S. T. Flock et al., "Optical properties of intralipid: a phantom medium for light propagation studies," *Laser Surg. Med.* **12**(5), 510–519 (1992).
13. A. Mazhar et al., "Structured illumination enhances resolution and contrast in thick tissue fluorescence imaging," *J. Biomed. Opt.* **15**(1), 010506 (2010).
14. S. Gioux et al., "Three-dimensional surface profile intensity correction for spatially modulated imaging," *J. Biomed. Opt.* **14**(3), 034045 (2009).